Beam Energy Dependence of Moments of the Net-Charge Multiplicity Distributions in Au + Au Collisions at RHIC

L. Adamczyk,[1] J. K. Adkins,[23] G. Agakishiev,[21] M. M. Aggarwal,[35] Z. Ahammed,[54] I. Alekseev,[19] J. Alford,[22] C. D. Anson,[32] A. Aparin,[21] D. Arkhipkin,[4] E. C. Aschenauer,[4] G. S. Averichev,[21] J. Balewski,[27] A. Banerjee,[54] Z. Barnovska,[14] D. R. Beavis,[4] R. Bellwied,[50] A. Bhasin,[20] A. K. Bhati,[35] P. Bhattarai,[49] H. Bichsel,[56] J. Bielcik,[13] J. Bielcikova,[14] L. C. Bland,[4] I. G. Bordyuzhin,[19] W. Borowski,[46] J. Bouchet,[22] A. V. Brandin,[30] S. G. Brovko,[6] S. Bültmann,[33] I. Bunzarov,[21] T. P. Burton,[4] J. Butterworth,[41] H. Caines,[57] M. Calderón de la Barca Sánchez,[6] D. Cebra,[6] R. Cendejas,[36] M. C. Cervantes,[48] P. Chaloupka,[13] Z. Chang,[48] S. Chattopadhyay,[54] H. F. Chen,[43] J. H. Chen,[45] L. Chen,[9] J. Cheng,[51] M. Cherney,[12] A. Chikanian,[57] W. Christie,[4] J. Chwastowski,[11] M. J. M. Codrington,[49] R. Corliss,[27] J. G. Cramer,[56] H. J. Crawford,[5] X. Cui,[43] S. Das,[16] A. Davila Leyva,[49] L. C. De Silva,[50] R. R. Debbe,[4] T. G. Dedovich,[21] J. Deng,[44] A. A. Derevschikov,[37] R. Derradi de Souza,[8] S. Dhamija,[18] B. di Ruzza,[4] L. Didenko,[4] C. Dilks,[36] F. Ding,[6] P. Djawotho,[48] X. Dong,[26] J. L. Drachenberg,[53] J. E. Draper,[6] C. M. Du,[25] L. E. Dunkelberger,[7] J. C. Dunlop,[4] L. G. Efimov,[21] J. Engelage,[5] K. S. Engle,[52] G. Eppley,[41] L. Eun,[26] O. Evdokimov,[10] R. Fatemi,[23] S. Fazio,[4] J. Fedorisin,[21] P. Filip,[21] E. Finch,[57] Y. Fisyak,[4] C. E. Flores,[6] C. A. Gagliardi,[48] D. R. Gangadharan,[32] D. Garand,[38] F. Geurts,[41] A. Gibson,[53] M. Girard,[55] S. Gliske,[2] D. Grosnick,[53] Y. Guo,[43] A. Gupta,[20] S. Gupta,[20] W. Guryn,[4] B. Haag,[6] O. Hajkova,[13] A. Hamed,[48] L-X. Han,[45] R. Haque,[31] J. W. Harris,[57] J. P. Hays-Wehle,[27] S. Heppelmann,[36] A. Hirsch,[38] G. W. Hoffmann,[49] D. J. Hofman,[10] S. Horvat,[57] B. Huang,[4] H. Z. Huang,[7] P. Huck,[9] T. J. Humanic,[32] G. Igo,[7] W. W. Jacobs,[18] H. Jang,[24] E. G. Judd,[5] S. Kabana,[46] D. Kalinkin,[19] K. Kang,[51] K. Kauder,[10] H. W. Ke,[9] D. Keane,[22] A. Kechechyan,[21] A. Kesich,[6] Z. H. Khan,[10] D. P. Kikola,[38] I. Kisel,[15] A. Kisiel,[55] D. D. Koetke,[53] T. Kollegger,[15] J. Konzer,[38] I. Koralt,[33] W. Korsch,[23] L. Kotchenda,[30] P. Kravtsov,[30] K. Krueger,[2] I. Kulakov,[15] L. Kumar,[31] R. A. Kycia,[11] M. A. C. Lamont,[4] J. M. Landgraf,[4] K. D. Landry,[7] J. Lauret,[4] A. Lebedev,[4] R. Lednicky,[21] J. H. Lee,[4] W. Leight,[27] M. J. LeVine,[4] C. Li,[43] W. Li,[45] X. Li,[38] X. Li,[47] Y. Li,[51] Z. M. Li,[9] L. M. Lima,[42] M. A. Lisa,[32] F. Liu,[9] T. Ljubicic,[4] W. J. Llope,[41] R. S. Longacre,[4] X. Luo,[9] G. L. Ma,[45] Y. G. Ma,[45] D. M. M. D. Madagodagettige Don,[12] D. P. Mahapatra,[16] R. Majka,[57] S. Margetis,[22] C. Markert,[49] H. Masui,[26] H. S. Matis,[26] D. McDonald,[41] T. S. McShane,[12] N. G. Minaev,[37] S. Mioduszewski,[48] B. Mohanty,[31] M. M. Mondal,[48] D. A. Morozov,[37] M. G. Munhoz,[42] M. K. Mustafa,[38] B. K. Nandi,[17] Md. Nasim,[31] T. K. Nayak,[54] J. M. Nelson,[3] L. V. Nogach,[37] S. Y. Noh,[24] J. Novak,[29] S. B. Nurushev,[37] G. Odyniec,[26] A. Ogawa,[4] K. Oh,[39] A. Ohlson,[57] V. Okorokov,[30] E. W. Oldag,[49] R. A. N. Oliveira,[42] M. Pachr,[13] B. S. Page,[18] S. K. Pal,[54] Y. X. Pan,[7] Y. Pandit,[10] Y. Panebratsev,[21] T. Pawlak,[55] B. Pawlik,[34] H. Pei,[9] C. Perkins,[5] W. Peryt,[55] A. Peterson,[32] P. Pile,[4] M. Planinic,[58] J. Pluta,[55] D. Plyku,[33] N. Poljak,[58] J. Porter,[26] A. M. Poskanzer,[26] N. K. Pruthi,[35] M. Przybycien,[1] P. R. Pujahari,[17] H. Qiu,[26] A. Quintero,[22] S. Ramachandran,[23] R. Raniwala,[40] S. Raniwala,[40] R. L. Ray,[49] C. K. Riley,[57] H. G. Ritter,[26] J. B. Roberts,[41] O. V. Rogachevskiy,[21] J. L. Romero,[6] J. F. Ross,[12] A. Roy,[54] L. Ruan,[4] J. Rusnak,[14] N. R. Sahoo,[54] P. K. Sahu,[16] I. Sakrejda,[26] S. Salur,[26] A. Sandacz,[55] J. Sandweiss,[57] E. Sangaline,[6] A. Sarkar,[17] J. Schambach,[49] R. P. Scharenberg,[38] A. M. Schmah,[26] W. B. Schmidke,[4] N. Schmitz,[28] J. Seger,[12] P. Seyboth,[28] N. Shah,[7] E. Shahaliev,[21] P. V. Shanmuganathan,[22] M. Shao,[43] B. Sharma,[35] W. Q. Shen,[45] S. S. Shi,[26] Q. Y. Shou,[45] E. P. Sichtermann,[26] R. N. Singaraju,[54] M. J. Skoby,[18] D. Smirnov,[4] N. Smirnov,[57] D. Solanki,[40] P. Sorensen,[4] U. G. deSouza,[42] H. M. Spinka,[2] B. Srivastava,[38] T. D. S. Stanislaus,[53] J. R. Stevens,[27] R. Stock,[15] M. Strikhanov,[30] B. Stringfellow,[38] A. A. P. Suaide,[42] M. Sumbera,[14] X. Sun,[26] X. M. Sun,[26] Y. Sun,[43] Z. Sun,[25] B. Surrow,[47] D. N. Svirida,[19] T. J. M. Symons,[26] A. Szanto de Toledo,[42] J. Takahashi,[8] A. H. Tang,[4] Z. Tang,[43] T. Tarnowsky,[29] J. H. Thomas,[26] A. R. Timmins,[50] D. Tlusty,[14] M. Tokarev,[21] S. Trentalange,[7] R. E. Tribble,[48] P. Tribedy,[54] B. A. Trzeciak,[55] O. D. Tsai,[7] J. Turnau,[34] T. Ullrich,[4] D. G. Underwood,[2] G. Van Buren,[4] G. van Nieuwenhuizen,[27] J. A. Vanfossen, Jr.,[22] R. Varma,[17] G. M. S. Vasconcelos,[8] A. N. Vasiliev,[37] R. Vertesi,[14] F. Videbæk,[4] Y. P. Viyogi,[54] S. Vokal,[21] A. Vossen,[18] M. Wada,[49] M. Walker,[27] F. Wang,[38] G. Wang,[7] H. Wang,[4] J. S. Wang,[25] X. L. Wang,[43] Y. Wang,[51] Y. Wang,[10] G. Webb,[23] J. C. Webb,[4] G. D. Westfall,[29] H. Wieman,[26] S. W. Wissink,[18] R. Witt,[52] Y. F. Wu,[9] Z. Xiao,[51] W. Xie,[38] K. Xin,[41] H. Xu,[25] N. Xu,[26] Q. H. Xu,[44] Y. Xu,[43] Z. Xu,[4] W. Yan,[51] C. Yang,[43] Y. Yang,[25] Y. Yang,[9] Z. Ye,[10] P. Yepes,[41] L. Yi,[38] K. Yip,[4] I-K. Yoo,[39] Y. Zawisza,[43] H. Zbroszczyk,[55] W. Zha,[43] J. B. Zhang,[9] S. Zhang,[45] X. P. Zhang,[51] Y. Zhang,[43] Z. P. Zhang,[43] F. Zhao,[7] J. Zhao,[45] C. Zhong,[45] X. Zhu,[51] Y. H. Zhu,[45] Y. Zoulkarneeva,[21] and M. Zyzak[15]

(STAR Collaboration)

[1]AGH University of Science and Technology, Cracow, Poland
[2]Argonne National Laboratory, Argonne, Illinois 60439, USA
[3]University of Birmingham, Birmingham, United Kingdom
[4]Brookhaven National Laboratory, Upton, New York 11973, USA
[5]University of California, Berkeley, California 94720, USA
[6]University of California, Davis, California 95616, USA
[7]University of California, Los Angeles, California 90095, USA
[8]Universidade Estadual de Campinas, Sao Paulo, Brazil
[9]Central China Normal University (HZNU), Wuhan 430079, China
[10]University of Illinois at Chicago, Chicago, Illinois 60607, USA
[11]Cracow University of Technology, Cracow, Poland
[12]Creighton University, Omaha, Nebraska 68178, USA
[13]Czech Technical University in Prague, FNSPE, Prague 115 19, Czech Republic
[14]Nuclear Physics Institute AS CR, 250 68 Řež/Prague, Czech Republic
[15]Frankfurt Institute for Advanced Studies FIAS, Germany
[16]Institute of Physics, Bhubaneswar 751005, India
[17]Indian Institute of Technology, Mumbai, India
[18]Indiana University, Bloomington, Indiana 47408, USA
[19]Alikhanov Institute for Theoretical and Experimental Physics, Moscow, Russia
[20]University of Jammu, Jammu 180001, India
[21]Joint Institute for Nuclear Research, Dubna 141 980, Russia
[22]Kent State University, Kent, Ohio 44242, USA
[23]University of Kentucky, Lexington, Kentucky 40506-0055, USA
[24]Korea Institute of Science and Technology Information, Daejeon, Korea
[25]Institute of Modern Physics, Lanzhou, China
[26]Lawrence Berkeley National Laboratory, Berkeley, California 94720, USA
[27]Massachusetts Institute of Technology, Cambridge, Massachusetts 02139-4307, USA
[28]Max-Planck-Institut für Physik, Munich, Germany
[29]Michigan State University, East Lansing, Michigan 48824, USA
[30]Moscow Engineering Physics Institute, Moscow, Russia
[31]National Institute of Science Education and Research, Bhubaneswar 751005, India
[32]Ohio State University, Columbus, Ohio 43210, USA
[33]Old Dominion University, Norfolk, Virginia 23529, USA
[34]Institute of Nuclear Physics PAN, Cracow, Poland
[35]Panjab University, Chandigarh 160014, India
[36]Pennsylvania State University, University Park, Pennsylvania 16802, USA
[37]Institute of High Energy Physics, Protvino, Russia
[38]Purdue University, West Lafayette, Indiana 47907, USA
[39]Pusan National University, Pusan, Republic of Korea
[40]University of Rajasthan, Jaipur 302004, India
[41]Rice University, Houston, Texas 77251, USA
[42]Universidade de Sao Paulo, Sao Paulo, Brazil
[43]University of Science & Technology of China, Hefei 230026, China
[44]Shandong University, Jinan, Shandong 250100, China
[45]Shanghai Institute of Applied Physics, Shanghai 201800, China
[46]SUBATECH, Nantes, France
[47]Temple University, Philadelphia, Pennsylvania 19122, USA
[48]Texas A&M University, College Station, Texas 77843, USA
[49]University of Texas, Austin, Texas 78712, USA
[50]University of Houston, Houston, Texas 77204, USA
[51]Tsinghua University, Beijing 100084, China
[52]United States Naval Academy, Annapolis, Maryland 21402, USA
[53]Valparaiso University, Valparaiso, Indiana 46383, USA
[54]Variable Energy Cyclotron Centre, Kolkata 700064, India
[55]Warsaw University of Technology, Warsaw, Poland
[56]University of Washington, Seattle, Washington 98195, USA
[57]Yale University, New Haven, Connecticut 06520, USA
[58]University of Zagreb, Zagreb HR-10002, Croatia

(Received 7 February 2014; revised manuscript received 24 July 2014; published 26 August 2014)

We report the first measurements of the moments—mean (M), variance (σ^2), skewness (S), and kurtosis (κ)—of the net-charge multiplicity distributions at midrapidity in Au + Au collisions at seven energies, ranging from $\sqrt{s_{NN}} = 7.7$ to 200 GeV, as a part of the Beam Energy Scan program at RHIC. The moments are related to the thermodynamic susceptibilities of net charge, and are sensitive to the location of the QCD critical point. We compare the products of the moments, σ^2/M, $S\sigma$, and $\kappa\sigma^2$, with the expectations from Poisson and negative binomial distributions (NBDs). The $S\sigma$ values deviate from the Poisson baseline and are close to the NBD baseline, while the $\kappa\sigma^2$ values tend to lie between the two. Within the present uncertainties, our data do not show nonmonotonic behavior as a function of collision energy. These measurements provide a valuable tool to extract the freeze-out parameters in heavy-ion collisions by comparing with theoretical models.

DOI: 10.1103/PhysRevLett.113.092301 PACS numbers: 25.75.-q, 12.38.Mh, 25.75.Gz, 25.75.Nq

The major goals of the physics program at Brookhaven National Laboratory's Relativistic Heavy-Ion Collider (RHIC) are the search for and study of a new form of matter known as the quark-gluon plasma (QGP) [1] and the mapping of the quantum chromodynamics (QCD) phase diagram in terms of temperature T and baryon chemical potential μ_B. Lattice QCD calculations indicate that at vanishing μ_B, the transition from the QGP to a hadron gas is a smooth crossover [2–8], while at large μ_B, the phase transition is of first order [4,9]. Therefore, a critical point in the QCD phase diagram is expected at finite μ_B, where the first order transition ends. The location of the critical point has been predicted to be accessible at RHIC [10–12], where the Beam Energy Scan program has been ongoing since 2010. The aim of this program is to map the QCD phase by varying the center-of-mass energy of the colliding ions, thereby scanning a large window in μ_B and T.

One of the characteristic signatures of the QCD critical point is the nonmonotonic behavior in the fluctuations of globally conserved quantities, such as the net-baryon, net-charge, and net-strangeness numbers, as a function of beam energy [4–8,10–19]. The event-by-event distributions of the conserved quantities within a limited acceptance are characterized by the moments, such as the mean (M), the standard deviation (σ), the skewness (S), which represents the asymmetry of the distribution, and the kurtosis (κ), which gives the degree to which the distribution is peaked relative to the normal distribution. These moments are related to the corresponding higher-order thermodynamic susceptibilities and to the correlation length of the system [19,20]. At the critical point, thermodynamic susceptibilities and the correlation length of the system are expected to diverge for large samples in equilibrium. But in reality, the phenomenon of critical slowing down in the vicinity of the critical point drives the system away from thermodynamic equilibrium, so the correlation length reaches a maximum value of around 1.5–3 fm [19,21]. Assuming that the signal at freeze-out survives dissipation during the evolution of the fireball from the hadronization stage [22], the higher moments can be used as one of the preferred tools for locating the critical point.

When relating the susceptibilities to the moments, a volume term appears, making it difficult to compare different systems and collision centralities. The products of the moments, such as σ^2/M, $S\sigma$, and $\kappa\sigma^2$, are constructed in order to cancel the volume term. Lattice QCD calculations have shown that these products go through rapid change near the critical point [4–7]. In addition, the products of the moments of the experimental data can be effectively used to determine the freeze-out points on the QCD phase diagram by comparing directly with first-principle lattice QCD calculations [23]. The net-charge multiplicity distributions are appropriate for all these studies as they directly probe a conserved quantum number [16–18]. Combining these results with the moments of net-proton multiplicity distributions [24], we may be able to extract the freeze-out parameters and probe the critical point.

In this Letter, we report the first measurements of the moments of the net-charge multiplicity distributions in Au + Au collisions at $\sqrt{s_{NN}} = 7.7$, 11.5, 19.6, 27, 39, 62.4, and 200 GeV, corresponding to μ_B from 410 to 20 MeV [25].

The data were taken by the Solenoid Tracker at RHIC (STAR) experiment in 2010 and 2011, as part of the Beam Energy Scan program at RHIC [12,13,26,27]. With large uniform acceptance and excellent particle identification capabilities, STAR provides an ideal environment for studying event-by-event distributions of charged particles. The Time Projection Chamber (TPC) [28] is the main tracking detector used to identify charged particles and obtain net charge (difference between the number of positive and negative charged particles) on an event-by-event basis. Combination of signals from the zero degree calorimeters [29], vertex position detectors [30], and beam-beam counters [31] are used as the minimum-bias trigger. The data analysis has been carried out for collisions occurring within ± 30 cm of the TPC center in the beam direction. Interactions of the beam with the beam pipe are rejected by selecting events with a radial vertex position in the transverse plane of less than 2 cm. The charged tracks are selected with more than 20 space points in the TPC out of 45, a distance of closest approach (DCA)

to the primary vertex of less than 1 cm, and the number of hit points used to calculate the specific energy loss greater than 10. The spallation protons, produced due to beam-pipe interactions, affect the charged particle measurement. These are suppressed by removing protons with transverse momentum p_T less than 400 MeV/c. To be consistent, antiprotons are also removed within this p_T range. The centrality of the collision is determined by using the total number of charged particles within a pseudorapidity η window of $0.5 < |\eta| < 1.0$, chosen to be beyond the analysis window of the net-charge distributions. The centrality is represented by the average number of participating nucleons $\langle N_{\rm part}\rangle$ as well as the percentage of total cross section, obtained by the Monte Carlo–Glauber simulation [32]. The total numbers of events analyzed are 1.4, 2.4, 15.5, 24, 56, 32, and 75(all $\times 10^6$) for $\sqrt{s_{NN}} = 7.7$, 11.5, 19.6, 27, 39, 62.4, and 200 GeV, respectively.

The measured positive (N_+) and negative (N_-) charged particle multiplicities within $|\eta| < 0.5$ and $0.2 < p_T < 2.0$ GeV/c (after removing protons and antiprotons with $p_T < 400$ MeV/c) are used to calculate net charge ($N_+ - N_-$) in each event. The net-charge distributions are obtained for different centrality classes. The finite centrality bin width may cause volume variations within a given centrality class and may introduce additional fluctuations. The moments and moments products are calculated at every integer value of the centrality variable. The values shown in the figures are weighted averages in 5% or 10% wide centrality bins, where the weights are the number of events at each value of the centrality variable normalized to unity within each such centrality bin. Such weighted averages effectively remove the dependence of the results on the width of the centrality bin [33,34]. The correction factor on the higher moments for choosing 5% or 10% wide centrality bins compared to narrower (1%) bins is about 2% or less.

Finite reconstruction efficiencies of the charged particles affect the measured moments. The efficiency for each centrality and collision energy is obtained by using the embedding technique [35]. The average efficiencies vary within 63%–66% and 70%–73% for most central (0%–5% bin) and peripheral (70%–80% bin) events, respectively, for all collision energies. The corrections to the moments are based on binomial probability distributions of efficiency [18]. For $\kappa\sigma^2$, the efficiency correction factors for all energies and centralities are consistent with unity, whereas for $S\sigma$, these factors vary from 1.4 to 1.0 from peripheral to central collisions for all energies.

The statistical errors of the moments and their products have been calculated using the Delta theorem approach [36] and Bootstrap method [37] for efficiency-uncorrected and efficiency-corrected results, respectively. The statistical uncertainties in the corrected results increase compared with the uncorrected ones because the efficiency corrections

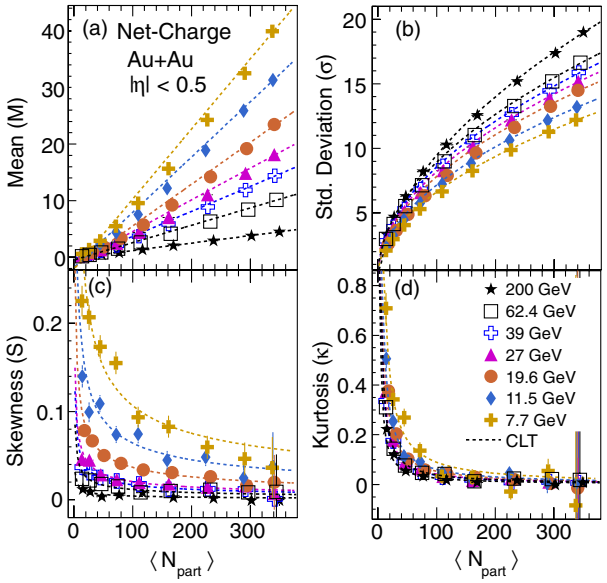

FIG. 1 (color online). The efficiency and centrality bin width corrected (a) mean, (b) standard deviation, (c) skewness, and (d) kurtosis of the net-charge multiplicity distributions as a function of number of participating nucleons $\langle N_{\rm part}\rangle$ for Au + Au collisions. The dotted lines represent calculations from the central limit theorem. The error bars are statistical and systematic errors are within the symbol sizes.

involve higher-order cumulants. The systematic uncertainties are obtained by varying the track selection criteria of the charged particles, such as the number of fit points, the DCA, and the number of hit points used to calculate ionization energy loss (dE/dx) in the TPC. The final systematic errors were estimated by including an additional 5% uncertainty in the reconstruction efficiency.

In Fig. 1, the efficiency and centrality bin width corrected moments of the net-charge distributions are plotted as a function of $\langle N_{\rm part}\rangle$ for Au + Au collisions at seven colliding energies. The statistical errors dominate in most cases and the systematic errors are within the symbol size. For all the collision energies, we observe that the M and σ values increase, whereas the S and κ values decrease with increasing $\langle N_{\rm part}\rangle$. The dotted lines in the figure are central limit theorem (CLT) calculations of the moments as a function of $\langle N_{\rm part}\rangle$ [38], which assume independent emission sources. These calculations follow the general trend of the data points. However, deviations from the CLT have been observed for several data points where the χ^2 values are as large as 16.9 for seven degrees of freedom. This may imply correlated emission of particles. The volume dependences of the moments are evident from Fig. 1, plotted as a function of $\langle N_{\rm part}\rangle$, which are canceled in suitably constructed products of the moments.

In order to understand the nature of the moments and their products, it is essential to compare the experimental results with baseline calculations. Two such calculations, one using the Poisson distribution and the other the

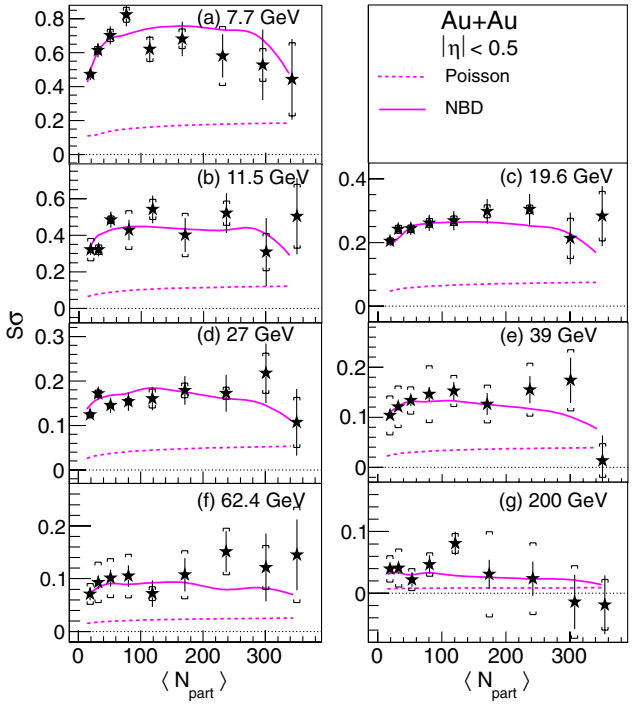

FIG. 2 (color online). Centrality dependence of $S\sigma$ in Au + Au collisions at $\sqrt{s_{NN}} = 7.7$ to 200 GeV. The results are efficiency and centrality bin width corrected. Results from the Poisson and NBD baselines are superimposed. The error bars are statistical and the caps represent systematic errors.

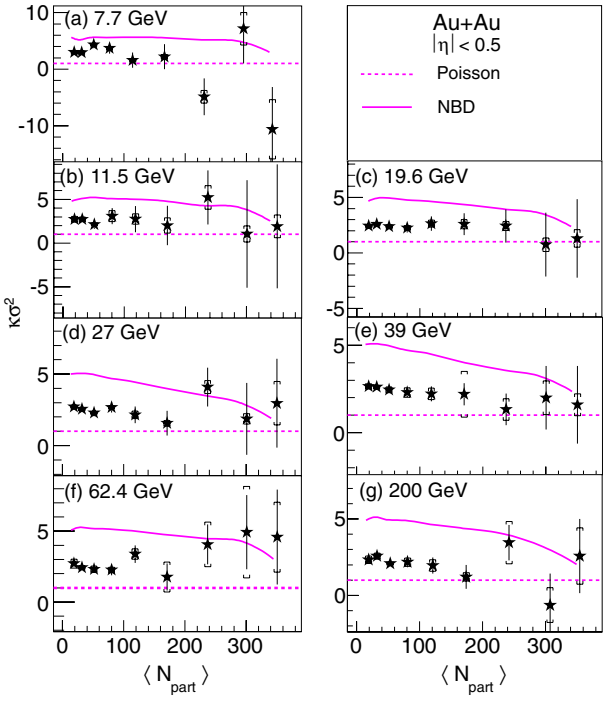

FIG. 3 (color online). Centrality dependence of $\kappa\sigma^2$ in Au + Au collisions at $\sqrt{s_{NN}} = 7.7$ to 200 GeV. The results are efficiency and centrality bin width corrected. Results from the Poisson and NBD baselines are superimposed. The error bars are statistical and the caps represent systematic errors.

negative binomial distribution (NBD), have been studied. In case of the Poisson baseline, the positive and negative charged particle multiplicities are randomly sampled from their mean values, resulting in a Skellam net-charge distribution [39]. The NBD baselines are constructed by using both the measured mean values and variances of the positive and negative charged particles [40]. Like the CLT, the Poisson and NBD baselines assume that the event by event multiplicities of positive and negative particles are independent random variables, i.e., completely uncorrelated. The Poisson and NBD assumptions result in different relationships between the moments of positive and negative particles. These baselines may provide adequate references for the moments of the net-charge distributions. Deviations from the baseline values, if any, would help us to observe possible nonmonotonic behavior.

Figures 2 and 3 show the values of $S\sigma$ and $\kappa\sigma^2$, respectively, plotted as functions of $\langle N_{\rm part}\rangle$ for Au + Au at seven collision energies. The data are corrected for centrality bin width effect and detector efficiencies. Results from Poisson and NBD baselines are superimposed in both figures. The $S\sigma$ values, shown in Fig. 2, systematically decrease with increasing beam energy for all centralities. The Poisson and NBD baselines are close to the data at $\sqrt{s_{NN}} = 200$ GeV. The differences between the baselines and the data increase with decreasing beam energy. For low energies ($\sqrt{s_{NN}} \leq 27$ GeV), the data are systematically above the Poisson baselines by more than 2 standard deviations, whereas the NBD baselines give a better description of the data. Figure 3 shows that the values of $\kappa\sigma^2$ at all energies and centralities are consistently larger than the Poisson baselines and below the NBD baselines. The NBD baselines are closer to the data than the Poisson baselines, but fail to quantitatively reproduce the experimental values. This is an indication of the existence of intraevent correlations of positive and negative charged particles in the data, even within the finite detector acceptance.

In Fig. 4, we compare the beam-energy dependence of σ^2/M, $S\sigma$, and $\kappa\sigma^2$ for two centrality bins, one corresponding to most central (0%–5% bin) and the other to peripheral (70%–80% bin) collisions. Results from the Poisson and NBD baselines are superimposed for both of the centralities. All of the results shown in this figure are efficiency and centrality bin width corrected. The values of σ^2/M increase with increasing beam energy, and are larger for peripheral collisions compared with the central collisions. In general, both the baseline calculations overestimate the data. The $S\sigma$ values are close to zero for $\sqrt{s_{NN}} = 200$ GeV, and increase with decreasing beam energy for both centralities. The Poisson baselines underestimate the $S\sigma$ values in most of cases, whereas the NBD baselines are closer to the data. The peripheral data are better described by the NBD baselines compared with the central data points. The $\kappa\sigma^2$

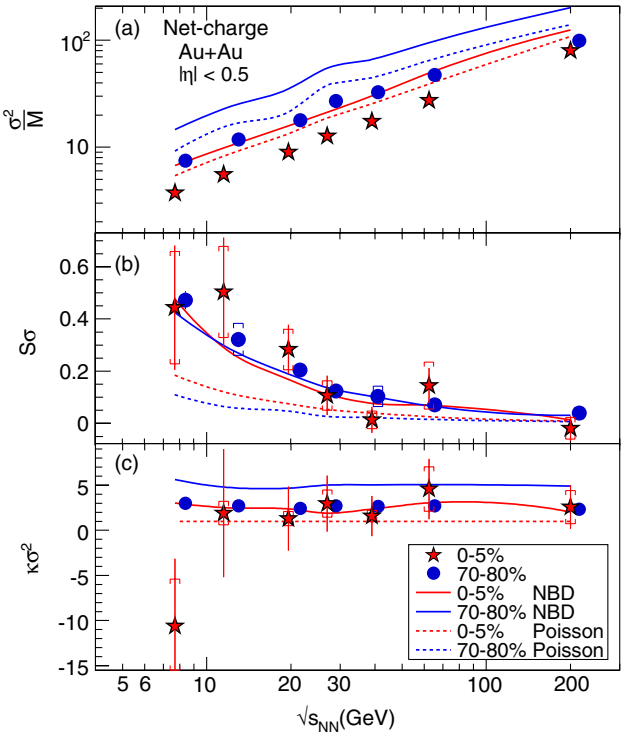

FIG. 4 (color online). Beam-energy dependence of (a) σ^2/M, (b) $S\sigma$, and (c) $\kappa\sigma^2$, after all corrections, for most central (0%–5%) and peripheral (70–80%) bins. The error bars are statistical and the caps represent systematic errors. Results from the Poisson and NBD baselines are superimposed. The values of $\kappa\sigma^2$ for the Poisson baseline are always unity.

values for the Poisson baselines are always unity. For peripheral collisions the $\kappa\sigma^2$ values show almost no variation as a function of beam energy and lie above the Poisson baseline and below the NBD baseline. For central collisions, within the statistical and systematic errors of the data, the $\kappa\sigma^2$ values at all energies are consistent with each other, except for $\sqrt{s_{NN}} = 7.7$ GeV. The weighted mean of $\kappa\sigma^2$ calculated for central collisions at all energies is 2.4 ± 1.2. For central collisions, both of the baseline calculations follow the data points except for the one at the lowest energy. Deviations of the data points with respect to the baseline calculations have been quantified in terms of the significance of deviation, defined as $(|\text{Data} - \text{Baseline}|)/(\sqrt{\text{err}^2_{\text{stat}} + \text{err}^2_{\text{sys}}})$, where err_{stat} and err_{sys} are the statistical and systematic errors, respectively. These deviations remain within 2 in the case of $S\sigma$ and $\kappa\sigma^2$ with respect to the corresponding Poisson and NBD baselines. This implies that the products of moments do not show nonmonotonic behavior as a function of beam energy.

The fluctuations of conserved quantities can be used to extract the thermodynamic information on chemical freeze-out by comparing experimentally measured higher moments with those from first-principle lattice QCD calculations [23]. Traditionally, by using the integrated hadron yields, the first moment of the fluctuations, the chemical freeze-out have been extracted from hadron resonance gas (HRG) models [25,41]. However, higher-order correlation functions should allow stricter tests on the thermal equilibrium in heavy-ion collisions. Calculations of freeze-out parameters based on preliminary experimental data on moments of net-charge distributions have been obtained [42,43]. From the latest lattice [44] and HRG analyses [45] using the STAR net-charge and net-proton results for central Au + Au collisions at 7.7 to 200 GeV, the extracted freeze-out temperatures range from 135 to 151 MeV and μ_B values range from 326 to 23 MeV. The errors in these calculations increase from 2% to 10% as a function of decreasing beam energy, which is mostly due to the statistical uncertainty in the experimental measurements. More details can be found in Refs. [44,45]. Note that this is the first time that the experimentally measured higher moments have been used to determine the chemical freeze-out conditions in high-energy nuclear collisions. The freeze-out temperatures obtained from the higher moments analysis are lower with respect to the traditional method [25,46]. This difference could indicate a higher sensitivity to freeze-out in the higher moments, which warrants further investigation.

In summary, the first results of the moments of net-charge multiplicity distributions for $|\eta| < 0.5$ as a function of centrality for Au + Au collisions at seven collision energies from $\sqrt{s_{NN}} = 7.7$ to 200 GeV are presented. These data can be used to explore the nature of the QCD phase transition and to locate the QCD critical point. We observe that the σ^2/M values increase monotonically with increasing beam energy. Weak centrality dependence is observed for both $S\sigma$ and $\kappa\sigma^2$ at all energies. The $S\sigma$ values increase with decreasing beam energy, whereas $\kappa\sigma^2$ values are uniform except at the lowest beam energy. Most of the data points show deviations from the Poisson baselines. The NBD baselines are closer to the data than the Poisson baselines, but do not quantitatively reproduce the data, implying the importance of intraevent correlations of the multiplicities of positive and negative particles in the data. Within the present uncertainties, no nonmonotonic behavior has been observed in the products of moments as a function of collision energy. The measured moments of net-charge multiplicity distributions provide unique information about the freeze-out parameters by directly comparing with theoretical model calculations. Future measurements with high statistics data will be needed for a precise determination of the freeze-out conditions and to make definitive conclusions regarding the critical point.

We thank M. Asakawa, R. Gavai, S. Gupta, F. Karsch, V. Koch, S. Mukherjee, K. Rajagopal, K. Redlich, and M. A. Stephanov for discussions related to this work. We thank the RHIC Operations Group and RCF at BNL, the NERSC Center at LBNL, the KISTI Center in Korea, and the Open Science Grid consortium for providing resources

and support. This work was supported in part by the Offices of NP and HEP within the U.S. DOE Office of Science, the U.S. NSF, CNRS/IN2P3, FAPESP CNPq of Brazil, the Ministry of Education and Science of the Russian Federation, NNSFC, CAS, MoST and MoE of China, the Korean Research Foundation, GA and MSMT of the Czech Republic, FIAS of Germany, DAE, DST, and CSIR of India, the National Science Centre of Poland, National Research Foundation (NRF-2012004024), the Ministry of Science, Education and Sports of the Republic of Croatia, and RosAtom of Russia.

[1] J. Adams *et al.* (STAR Collaboration), Nucl. Phys. **A757**, 102 (2005).
[2] Y. Aoki, G. Endrődi, Z. Fodor, S. D. Katz, and K. K. Szabó, Nature (London) **443**, 675 (2006).
[3] E. S. Bowman and J. I. Kapusta, Phys. Rev. C **79**, 015202 (2009).
[4] S. Ejiri, Phys. Rev. D **78**, 074507 (2008).
[5] Z. Fodor and S. D. Katz, J. High Energy Phys. 04 (2004) 050.
[6] R. V. Gavai and S. Gupta, Phys. Rev. D **78**, 114503 (2008).
[7] M. Cheng *et al.*, Phys. Rev. D **77**, 014511 (2008).
[8] M. A. Stephanov, Prog. Theor. Phys. Suppl. **153**, 139 (2004); Int. J. Mod. Phys. A **20**, 4387 (2005).
[9] C. Herold, M. Nahrgang, I. Mitshustin, and M. Bleicher, Nucl. Phys. **A925**, 14 (2014).
[10] M. A. Stephanov, K. Rajagopal, and E. V. Shuryak, Phys. Rev. Lett. **81**, 4816 (1998).
[11] M. A. Stephanov, K. Rajagopal, and E. V. Shuryak, Phys. Rev. D **60**, 114028 (1999).
[12] M. M. Aggarwal *et al.* (STAR Collaboration), arXiv: 1007.2613.
[13] M. M. Aggarwal *et al.* (STAR Collaboration), Phys. Rev. Lett. **105**, 022302 (2010).
[14] P. Braun-Munzinger, B. Friman, F. Karsch, K. Redlich, and V. Skokov, Nucl. Phys. **A880**, 48 (2012).
[15] M. Asakawa, S. Ejiri, and M. Kitazawa, Phys. Rev. Lett. **103**, 262301 (2009).
[16] V. Skokov, B. Friman, and K. Redlich, Phys. Lett. B **708**, 179 (2012).
[17] M. Kitazawa and M. Asakawa, Phys. Rev. C **85**, 021901 (2012).
[18] A. Bzdak and V. Koch, Phys. Rev. C **86**, 044904 (2012).
[19] C. Athanasiou, K. Rajagopal, and M. Stephanov, Phys. Rev. D **82**, 074008 (2010).
[20] M. A. Stephanov, Phys. Rev. Lett. **102**, 032301 (2009).
[21] B. Berdnikov and K. Rajagopal, Phys. Rev. D **61**, 105017 (2000).
[22] M. A. Stephanov, Phys. Rev. D **81**, 054012 (2010).
[23] A. Bazavov *et al.*, Phys. Rev. Lett. **109**, 192302 (2012).
[24] L. Adamczyk *et al.* (STAR Collaboration), Phys. Rev. Lett. **112**, 032302 (2014).
[25] J. Cleymans, H. Oeschler, K. Redlich, and S. Wheaton, Phys. Rev. C **73**, 034905 (2006).
[26] D. McDonald, Ph.D. thesis, Rice University, 2013.
[27] N. R. Sahoo, Ph.D. thesis, Homi Bhabha National Institute, 2013.
[28] M. Anderson *et al.*, Nucl. Instrum. Methods Phys. Res., Sect. A **499**, 659 (2003).
[29] C. Adler, A. Denisov, E. Garcia, M. Murray, H. Stroebele, and S. White, Nucl. Instrum. Methods Phys. Res., Sect. A **470**, 488 (2001).
[30] W. J. Llope *et al.*, Nucl. Instrum. Methods Phys. Res., Sect. A **522**, 252 (2004).
[31] C. A. Whitten, AIP Conf. Proc. **980**, 390 (2008).
[32] M. L. Miller, K. Reygers, S. J. Sanders, and P. Steinberg, Annu. Rev. Nucl. Part. Sci. **57**, 205 (2007).
[33] X. Luo, J. Xu, B. Mohanty, and N. Xu, J. Phys. G **40**, 105104 (2013).
[34] N. R. Sahoo, S. De, and T. K. Nayak, Phys. Rev. C **87**, 044906 (2013).
[35] B. I. Abelev *et al.* (STAR Collaboration), Phys. Rev. C **79**, 034909 (2009).
[36] X. Luo, J. Phys. G **39**, 025008 (2012).
[37] B. Efron and R. J. Tibshirani, *An introduction to the bootstrap* (Chapman & Hall/CRC, London, 1993).
[38] According to the central limit theorem, M, σ^2, S, and κ are proportional to $\langle N_{\rm part}\rangle$, $\sqrt{\langle N_{\rm part}\rangle}$, $1/\sqrt{\langle N_{\rm part}\rangle}$, and $1/\langle N_{\rm part}\rangle$, respectively.
[39] The difference of two independent Poisson distributions is a Skellam distribution, for which $\sigma^2/M = (\langle N_+\rangle + \langle N_-\rangle)/\langle N_+\rangle - \langle N_-\rangle$, $S\sigma = (\langle N_+\rangle - \langle N_-\rangle)/\langle N_+\rangle + \langle N_-\rangle$, and $\kappa\sigma^2 = 1$.
[40] T. J. Tarnowsky and G. D. Westfall, Phys. Lett. B **724**, 51 (2013).
[41] A. Andronic *et al.*, Nucl. Phys. **A837**, 65 (2010).
[42] S. Mukherjee and M. Wagner, *Proc. Sci.*, CPOD2013 (2013) 039.
[43] S. Borsányi, Z. Fodor, S. D. Katz, S. Krieg, C. Ratti, and K. K. Szabó, Phys. Rev. Lett. **111**, 062005 (2013).
[44] S. Borsanyi, Z. Fodor, S. D. Katz, S. Krieg, C. Ratti, and K. K. Szabo, Phys. Rev. Lett. **113**, 052301 (2014).
[45] P. Alba *et al.*, arXiv:1403.4903.
[46] L. Kumar, *Proc. Sci.*, CPOD2013 (2013) 047.